JOURNAL OF BACTERIOLOGY, Mar. 2006, p. 1856–1865 Vol. 188, No. 5
0021-9193/06/$08.00+0 doi:10.1128/JB.188.5.1856–1865.2006

Mycobacterium tuberculosis Cells Growing in Macrophages Are Filamentous and Deficient in FtsZ Rings

Ashwini Chauhan,[1] Murty V. V. S. Madiraju,[1] Marek Fol,[1] Hava Lofton,[1] Erin Maloney,[1] Robert Reynolds,[2] and Malini Rajagopalan[1]*

Biomedical Research, The University of Texas Health Center at Tyler, Tyler, Texas 75708-3154,[1] and Drug Discovery Division, Southern Research Institute, Birmingham, Alabama 35205[2]

Received 8 November 2005/Accepted 12 December 2005

FtsZ, a bacterial homolog of tubulin, forms a structural element called the FtsZ ring (Z ring) at the predivisional midcell site and sets up a scaffold for the assembly of other cell division proteins. The genetic aspects of FtsZ-catalyzed cell division and its assembly dynamics in *Mycobacterium tuberculosis* are unknown. Here, with an *M. tuberculosis* strain containing $FtsZ_{TB}$ tagged with green fluorescent protein as the sole source of FtsZ, we examined FtsZ structures under various growth conditions. We found that midcell Z rings are present in approximately 11% of actively growing cells, suggesting that the low frequency of Z rings is reflective of their slow growth rate. Next, we showed that SRI-3072, a reported $FtsZ_{TB}$ inhibitor, disrupted Z-ring assembly and inhibited cell division and growth of *M. tuberculosis*. We also showed that *M. tuberculosis* cells grown in macrophages are filamentous and that only a small fraction had midcell Z rings. The majority of filamentous cells contained nonring, spiral-like FtsZ structures along their entire length. The levels of FtsZ in bacteria grown in macrophages or in broth were comparable, suggesting that Z-ring formation at midcell sites was compromised during intracellular growth. Our results suggest that the intraphagosomal milieu alters the expression of *M. tuberculosis* genes affecting Z-ring formation and thereby cell division.

Mycobacterium tuberculosis, the causative agent of tuberculosis, is an important infectious agent that globally causes more than three million new infections each year (8). Recent years have seen an increase in the number of *M. tuberculosis* strains that are resistant to one or more antituberculosis drugs, and this has highlighted the need for the development of a new generation of antimicrobial agents. One hallmark of the *M. tuberculosis* life cycle is that it exists in two metabolically distinct growth states: an active replicative state and a nonproliferative persistent state where the bacterium survives without any increase in the bacterial burden on the host. Physiological studies carried out by Wayne and colleagues indicate that *M. tuberculosis* cells in the hypoxia-induced nonreplicative persistent state are blocked at the cell division stage after completing DNA replication and undergo a round of cell division prior to initiation of a new round of DNA replication (40, 41). This latter process is also referred to as reactivation. Development of antimycobacterial agents targeting the cell division process could potentially prevent the multiplication and subsequent proliferation of the pathogen in active, as well as reactivation, growth states.

FtsZ, a bacterial homolog of tubulin, is a key player in cell division and is essential for initiation of this process (22, 32). FtsZ protein catalyzes the formation of distinct structures, referred to as FtsZ rings (Z rings), at the midcell site and sets up a scaffold for ordered assembly of other cell division proteins. The combined action of multiple cell division proteins results in septation (22, 32). FtsZ protein-catalyzed Z-ring assembly represents the earliest known step in the septation process. FtsZ protein polymerizes in vitro into protofilaments in a GTP-dependent manner, and its assembly dynamics are regulated by GTP hydrolysis (25). FtsZ is a well-conserved protein that is present in nearly all prokaryotes (22). Due to its central and essential role in bacterial cytokinesis, and its absence in higher eukaryotes, the FtsZ protein is considered an attractive antimicrobial drug target (3, 19, 21, 22, 25, 44).

Earlier studies on *ftsZ* and the cell division process in mycobacteria focused on *Mycobacterium smegmatis*, a rapid grower with an average doubling time of 3 h. These studies indicated that *ftsZ* is an essential cell division gene (10) and that *M. tuberculosis* is exquisitely sensitive to the intracellular levels of FtsZ ($FtsZ_{TB}$), as constructs expressing $ftsZ_{TB}$ from native or heterologous promoters are not stably maintained (9). Because of the toxicity associated with elevated expression levels of *ftsZ* in *M. tuberculosis*, attempts to visualize FtsZ structures in *M. tuberculosis* have not been successful. At the biochemical level, $FtsZ_{TB}$ has been purified, characterized, and found to exhibit slow polymerization and weak GTPase activities in vitro (30, 43).

We have been unable to localize FtsZ structures in mycobacteria by immunohistochemistry due, perhaps, to their thick and unyielding cell walls (9). This feature, combined with the toxicity associated with the elevated levels of $ftsZ_{TB}$ expression in *M. tuberculosis*, led us to develop an $ftsZ_{TB}$ reporter strain where FtsZ-green fluorescent protein (GFP) fusion protein can function as the sole source of FtsZ (10). With this strain, we visualized $FtsZ_{TB}$ structures in *M. tuberculosis* grown under different conditions. We describe here the FtsZ localization in cells growing in culture and in macrophages.

* Corresponding author. Mailing address: Biomedical Research, The University of Texas Health Center at Tyler, Tyler, TX 75708-3154. Phone: (903) 877-7731. Fax: (903) 877-5969. E-mail: malini.rajagopalan@uthct.edu.

MATERIALS AND METHODS

Bacterial growth conditions and survival studies. *Escherichia coli* Top10, used for cloning, was propagated in Luria-Bertani broth, and transformants were

TABLE 1. Plasmids used in this study

Plasmid	Description	Reference
pGOAL17	Carrying 6.1-kb PacI cassette, Km^r	27
p2NIL	Nonreplicating recombination vector, Km^r	27
pMV306H	Mycobacterial integrating vector, Hyg^r	Med-Immune Inc.
pMV306K	Mycobacterial integrating vector, Km^r	Med-Immune Inc.
pMV206	*E. coli-Mycobacterium* shuttle vector, Km^r	Med-Immune Inc.
pJFR19	3-kb amidase promoter in pMV306H, Hyg^r	This study
pJFR51	p2NIL containing 3.6-kb *ftsZ*$_{TB}$ region with 840-bp internal deletion in *ftsZ* coding region, Km^r	This study
pJFR52	pJFR51 with PacI cassette from pGOAL17, Km^r	This study
pJFR66	pMV306H carrying *PftsZ-ftsZ*$_{TB}$, Hyg^r	This study
pJFR41	*ftsZ*$_{TB}$*-gfp* in pJFR19, Hyg^r	This study
pACR1	pMV306K carrying *PftsZ-ftsZ*$_{smeg}$, Km^r	This study

selected on Luria-Bertani agar containing either kanamycin (Km, 50 μg/ml) or hygromycin (Hyg, 50 μg/ml). *M. smegmatis* mc^2-155 and *M. tuberculosis* H37Ra (and H37Rv) were grown in Middlebrook 7H9 broth supplemented with oleic acid, albumin, dextrose, and sodium chloride. Transformants were selected in the same medium supplemented with agar containing Km (10 μg/ml), Hyg (50 μg/ml), or both (10). As needed, acetamide was supplied in growth medium at a final concentration of 0.2%. In some experiments, actively growing cultures of *M. tuberculosis* were exposed to the small-molecule inhibitor SRI-3072 at 0.5 μM (about equal to the MIC). Growth was followed for several days after exposure by monitoring absorbance at 600 nm, and viability was measured by determining CFU.

Construction of *ftsZ* expression plasmids pACR1, pJFR41, and pJFR66. Plasmids pACR1 and pJFR66 were created by cloning the PCR-amplified fragments encompassing the *ftsZ*$_{smeg}$ and *ftsZ*$_{TB}$ coding regions and their respective 1-kb 5′ flanking regions (Table 1) in integrating plasmids. Plasmid pJFR41 was created by cloning the *ftsZ*$_{TB}$*-gfp* fusion (9) downstream of the amidase promoter in pJFR19 (Table 1). The *gfp* gene in pJFR41 was derived from the fluorescence-activated cell sorter-optimized mut3 variant amplified from pFV25 (5, 9). All PCR products were confirmed by sequencing.

Construction of suicide recombination substrates. A suicide recombination plasmid, pJFR52, containing the 3.6-kb *ftsZ*$_{TB}$ gene region with an 840-bp internal deletion in the *ftsZ*$_{TB}$ gene was constructed in two steps. First, a 2.1-kb DNA fragment bearing the 5′ end of *ftsZ*$_{TB}$ and its upstream flanking region and a 1.6-kb fragment bearing the 3′ end of *ftsZ*$_{TB}$ and its downstream flanking region, were amplified by using oligonucleotide primer pair MVM276 and MVM238 and pair MVM280 and MVM281, respectively (Table 2). The resultant PCR products were cloned adjacent to each other in vector p2NIL to create pJFR51 (27). Next, a 6.1-kb PacI fragment carrying the *lacZ*, *aph*, and *sacB* genes was isolated from pGOAL17 and inserted into pJFR51 to create suicide recombination plasmid pJFR52 (27).

Construction of an *ftsZ-gfp* mutant strain. The pJFR52 plasmid was electroporated into *M. tuberculosis* H37Ra, and single crossovers were selected on agar plates containing Km and 5-bromo-4-chloro-3-indolyl-β-D-galactopyranoside. A blue, Km-resistant single-crossover strain, *M. tuberculosis* 52, was confirmed by PCR. To inactivate *ftsZ* at its native location, a plasmid construct (pJFR66 in Table 1; Fig. 1) expressing *ftsZ* from its native promoter was integrated at the bacteriophage attachment site of *M. tuberculosis* 52, and the resultant merodiploid strain was screened for double crossovers (DCOs) as previously described (10). White, Km-sensitive, Hyg^r, and sucrose-resistant DCO colonies were analyzed by PCR and Southern hybridization with *ftsZ*$_{TB}$-specific, ^{32}P-labeled probes. One strain, designated *M. tuberculosis* 66, was confirmed to be chromosomally null for *ftsZ* and contained an integrated copy of *PftsZ-ftsZ*$_{TB}$. Integration at the *attB* site in mycobacteria can be efficiently excised by phage excisionase and replaced simultaneously with the incoming plasmid carrying alternate antibiotic markers (28). With this strategy, we switched the integrated plasmid expressing *ftsZ* from its native promoter (pJFR66, Hyg^r) by transforming the *M. tuberculosis* 66 strain with a KM resistance-encoding incoming plasmid expressing *PftsZ-ftsZ*$_{smeg}$, pACR1 (Table 1), to generate *M. tuberculosis* ACR1. Next, we swapped the resident plasmid in *M. tuberculosis* ACR1 with pJFR41 (*PamiftsZ*$_{TB}$*-gfp*, Hyg^r) to create *M. tuberculosis* 41. Inclusion of the pACR1 swapping step was necessary to generate *M. tuberculosis* 41, as both pJFR66 and pJFR41 carried a gene for Hyg^r, which would have made the screening process cumbersome. Since pACR1 expressed *M. smegmatis ftsZ*, these results also indicated that the *M. smegmatis* counterpart could substitute *ftsZ*$_{TB}$ function. Transformants with pJFR41 were plated on agar containing 0.2% acetamide. The DCO strains were confirmed by PCR amplification and sequencing of the integrated copy of the gene and by Southern hybridization with *ftsZ*$_{TB}$ and *gfp* gene-specific probes.

Southern hybridization. *M. tuberculosis* genomic DNA was isolated from various strains, digested with XhoI, and processed for Southern hybridization as previously described (33). Nitrocellulose blots were hybridized with PCR-generated, ^{32}P-labeled *ftsZ*$_{TB}$ (Table 2) and *gfp* (Table 2) probes (10).

Immunoblotting experiments. Immunoblotting was carried out to detect FtsZ$_{TB}$ and FtsZ$_{TB}$-GFP in cellular lysates of broth- and in vivo-grown wild-type *M. tuberculosis* and *M. tuberculosis* 41 as previously described (10). We used *M. tuberculosis* SigA protein to normalize for protein amounts loaded per lane when comparing the FtsZ levels in broth- and macrophage-grown *M. tuberculosis*. SigA levels are not known to change during intracellular growth of *M. tuberculosis* (45). Blots were probed simultaneously with anti-FtsZ$_{TB}$ antibodies and monoclonal antibodies to the sigma 70 subunit of *E. coli* RNA polymerase. The latter have been shown to bind mycobacterial SigA protein (29, 45). Anti-sigma 70 antibodies were obtained from Neoclone Biotechnology (Madison, WI) and used as recommended. Immunoblots were processed with the ECF Western blotting kit from Amersham (Piscataway, NJ) and scanned on a Bio-Rad Molecular Imager (FX), and FtsZ levels were determined with the volume analysis function of the QuantityOne software.

Fluorescence microscopy experiments. Wild-type *M. tuberculosis* and *M. tuberculosis* 41 were grown for various periods of time with shaking, harvested by centrifugation, washed in phosphate-buffered saline, fixed in 1% paraformaldehyde, and stored at 4°C until further use. Bacteria were examined by bright-field and fluorescence microscopy with a Nikon Eclipse 600 microscope equipped with a 100× Nikon Plan Fluor oil immersion objective with a numerical aperture of 1.4 and a standard fluorescein isothiocyanate filter set (Chroma). Images were acquired with a Photometrics Coolsnap ES camera and Metapmorph 6.2 imaging software (Universal Imaging Corporation). Images were optimized with Adobe Photoshop 7.0. Some images were processed with the homomorphic fast Fourier transform (FFT) filtering function of the Metamorph 6.2 software. When applied to an image, this function performs simultaneous contrast enhancement and compression of the brightness dynamic range.

Macrophage infection experiments. Monocyte-derived human macrophage cell line THP-1 was infected with either *M. tuberculosis* or *M. tuberculosis* 41. Uninfected THP-1 cells were maintained in RPMI medium with 10% fetal bovine serum. Prior to infection, THP-1 cells were exposed to 50 nM phorbol-12-myristate-13-acetate for 24 h and allowed to differentiate into macrophages. Approximately 5×10^5 cells/ml were infected with *M. tuberculosis* or *M. tuberculosis* 41 at a multiplicity of infection of 1:10 (macrophage/bacterium ratio). After 3 h of phagocytosis, macrophages were washed to remove nonphagocytosed bacteria and further incubated. At the indicated time points, either the

TABLE 2. Primes used in this study

Oligonucleotide	Sequence	Description
MVM187	5′-TTT GTA TAG TTC ATC C-3′	Reverse primer for *gfp*
MVM238	5′-GCG GAT CCG CTT CCT CCC TGG TGG GGC-3′	Binds 8 nucleotides upstream of *ftsZ*$_{TB}$
MVM276	5′-GCT CTA GAG TGA GCA CCG AGC AGT TGC C-3′	Binds 2.5 kb upstream of *ftsZ*$_{TB}$
MVM278	5′-GCG GAT CCG CGA CCG ATC CGC CAC CG-3′	Binds 1 kb upstream of *ftsZ*$_{TB}$
MVM280	5′-GCG GAT CCG TCG ATC GCC GGC GGC AGC-3′	Binds 3′ end of *ftsZ*$_{TB}$
MVM281	5′-GCC ATC TTG GCT GAA GCT TCC-3′	Binds 1.1 kb downstream of *ftsZ*$_{TB}$
MVM469	5′-TAA AGG AGA AGA ACT TTT CAC T-3′	Forward primer for *gfp*
MVM494	5′-GCC ACC ACC GAT ACC CAC GA-3′	Binds 5′ end of *ftsZ*$_{TB}$

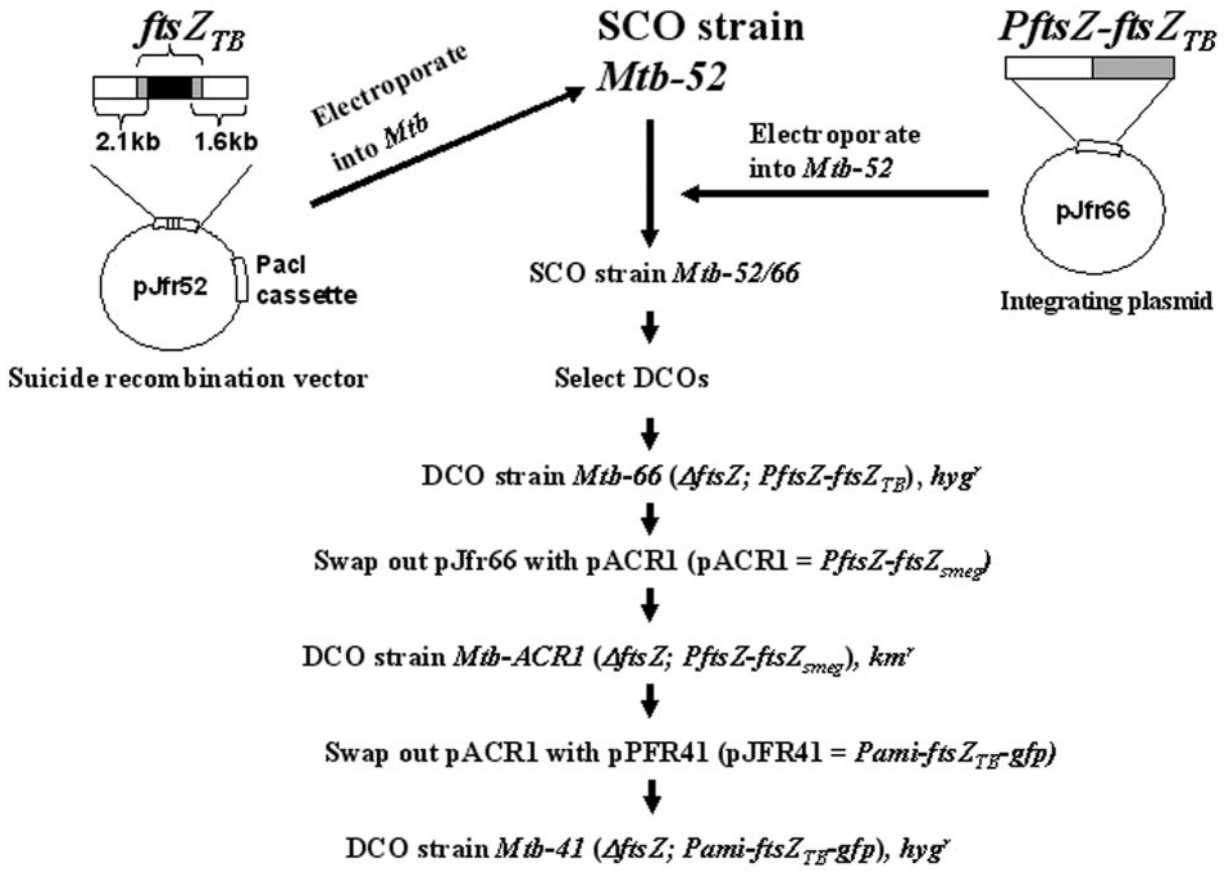

FIG. 1. Schematic for construction of *M. tuberculosis* 41. Plasmids are described in Table 1, and details for creating *M. tuberculosis* 41 are described in the text. Gray box, $ftsZ_{TB}$ coding region; black box, deleted region in $ftsZ_{TB}$; white box, 5′ and 3′ flanking regions of $ftsZ_{TB}$. SCO, single-crossover; *Mtb*, *M. tuberculosis*.

macrophages were lysed with 0.09% sodium dodecyl sulfate (SDS) and bacteria recovered following centrifugation at 14,000 rpm for 5 min or the infected macrophage monolayers were washed three times with phosphate-buffered saline, scraped, and resuspended in Tris-EDTA buffer. The recovered bacteria or macrophages containing bacteria were lysed by bead beating for 3 min in a mini bead beater. Cleared lysates were obtained by centrifugation, separated on SDS-polyacrylamide (PA), transferred to nitrocellulose, and probed for FtsZ levels as outlined above. For microscopy, the recovered bacteria were fixed in 1% paraformaldehyde and visualized by bright-field or fluorescence microscopy, as needed.

RESULTS AND DISCUSSION

Our approach to study $FtsZ_{TB}$-mediated cell division in *M. tuberculosis* is to construct an *ftsZ-gfp* mutant strain and investigate $FtsZ_{TB}$ ring assembly under different growth conditions. Our earlier studies revealed that self-replicating plasmid constructs expressing $ftsZ_{TB}$ in *M. tuberculosis* from either native or heterologous promoters are unstable (9). Also, intense fluorescent $FtsZ_{TB}$ structures in *M. smegmatis* merodiploids can be visualized if $FtsZ_{TB}$ is produced from the amidase promoter (*Pami-*$ftsZ_{TB}$*-gfp*) but not from its native promoter (*PftsZ-*$ftsZ_{TB}$*-gfp*) (9, 30). Bearing these two data in mind, we constructed an $ftsZ_{TB}$ reporter strain in which $FtsZ_{TB}$ tagged with GFP was the sole source of FtsZ (see below). Once constructed, the strain was characterized with respect to FtsZ levels, FtsZ structures, and growth in broth and macrophages.

We used the two-step recombination protocol of Parish and Stoker to disrupt the native *ftsZ* gene in the presence of an integrated copy of $ftsZ_{TB}$ (27). Mapping of $ftsZ_{TB}$ transcriptional start points identified four promoters, with the farthest one at 787 nucleotides upstream of the $ftsZ_{TB}$ start codon (data not shown). Accordingly, a DNA fragment bearing the $ftsZ_{TB}$ coding region and its 1-kb upstream flanking region was amplified, cloned in integrating vector pMV306H (pJFR66 in Table 1), and used during the selection of DCOs as described in Materials and Methods. One mutant DCO, designated *M. tuberculosis* 66 and carrying a functional copy of $ftsZ_{TB}$ at the *attB* site, was selected and used as the base strain to generate the $ftsZ_{TB}$*-gfp* reporter strain (*M. tuberculosis* 41) by a plasmid-swapping protocol (Fig. 1 and Materials and Methods) (28, 30). Southern hybridization of *M. tuberculosis* 41 genomic DNA with the *ftsZ* gene probe identified two bands: one corresponding to the integrated *ftsZ* copy and the other to the mutant copy carrying an 840-bp internal deletion in the $ftsZ_{TB}$ gene (Fig. 2A). A parallel blot hybridized with the *gfp* gene probe identified only one band corresponding to the integrated copy (Fig. 2B). These results confirmed that the transforma-

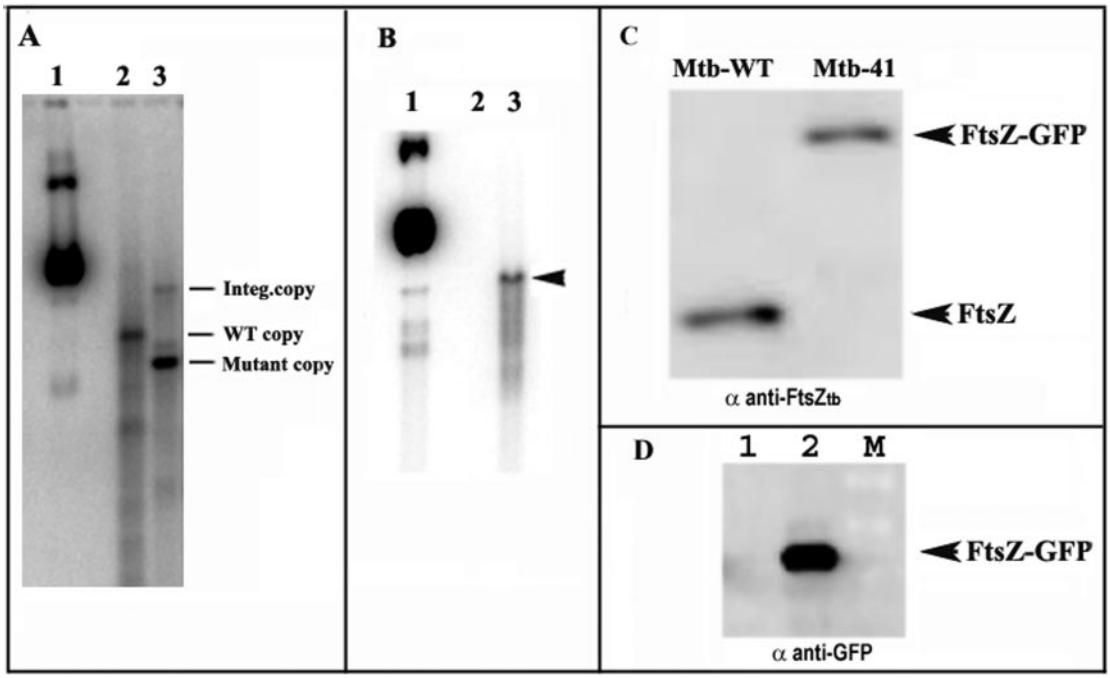

FIG. 2. *M. tuberculosis ftsZ* gene can be replaced with *ftsZ-gfp*. (A and B) Southern hybridization profiles of *M. tuberculosis* 41 and wild-type (WT) *M. tuberculosis* DNAs. Wild-type *M. tuberculosis* or *M. tuberculosis* 41 genomic DNA was digested with NotI, electrophoretically resolved on agarose gels, transferred to nitrocellulose membranes, and probed with a ^{32}P-labeled *ftsZ* (A) or *gfp* probe (B). NotI-digested pJFR41 plasmid DNA was used as a positive control. Lanes: 1, pJFR41; 2, wild-type *M. tuberculosis*; 3, *M. tuberculosis* 41. Bands corresponding to a chromosomal copy of *ftsZ* (wild-type copy), an integrated copy of *ftsZ-gfp* (Integ.copy), and a mutant copy are indicated. Only the wild-type copy of *ftsZ* can be seen in *M. tuberculosis*. The arrowhead indicates the position of the *ftsZ-gfp* integrated copy. (C and D) Verification of *M. tuberculosis* 41 by immunoblotting. One microgram of total cell lysate each from wild-type *M. tuberculosis* or *M. tuberculosis* 41 was resolved on a 12% SDS-PA gel, transferred to nitrocellulose membrane, and probed with either anti-FtsZ (C) or anti-GFP (D) specific antibodies. Positions of FtsZ and FtsZ-GFP are marked. Lanes: M, markers; 1, *M. tuberculosis* lysate; 2, *M. tuberculosis* 41 lysate.

tion-based plasmid-switching protocols successfully replaced the resident plasmid carrying *PftsZ-ftsZ*$_{TB}$ with an incoming plasmid containing *Pami-ftsZ*$_{TB}$*-gfp*.

Characterization of *M. tuberculosis ftsZ-gfp* reporter strain. To further validate the Southern data, *M. tuberculosis* 41 grown in the presence of 0.2% acetamide was examined for FtsZ$_{TB}$-GFP production by immunoblotting with anti-FtsZ$_{TB}$ and anti-GFP antibodies. When probed with anti-FtsZ$_{TB}$ antibodies, a distinct band corresponding to FtsZ-GFP fusion protein (65 kDa) and none corresponding to FtsZ$_{TB}$ (39 kDa) was detected in *M. tuberculosis* 41 lysates (Fig. 2C), whereas a 39-kDa band corresponding to FtsZ$_{TB}$ was detected in the lysates of wild-type *M. tuberculosis* (Fig. 2C). A parallel blot probed with anti-GFP antibodies revealed only one band corresponding to FtsZ$_{TB}$-GFP in *M. tuberculosis* 41 lysates and none in the parent strain *M. tuberculosis* (Fig. 2D, compare lane 2 with lane 1). Quantification of FtsZ and FtsZ-GFP bands in Fig. 2C revealed that the levels of FtsZ-GFP fusion protein in *M. tuberculosis* 41 were comparable to those of the native protein produced in the parent strain (the ratio of FtsZ-GFP to FtsZ was 0.9:1) (Fig. 2C). It is interesting that expression of *ftsZ*$_{TB}$*-gfp* from the amidase promoter in self-replicating plasmids in *M. smegmatis* resulted in the accumulation of excess fusion protein (12, 15). Thus, the nearly normal levels of FtsZ$_{TB}$-GFP in *M. tuberculosis* 41 cells suggest that FtsZ$_{TB}$ levels in *M. tuberculosis* are more tightly regulated than in *M. smegmatis*.

The viability of *M. tuberculosis* 41 decreased by nearly 5 log units when actively growing cultures were plated on medium lacking acetamide (Fig. 3A). The growth rate of *M. tuberculosis* 41, slightly slower than that of wild-type *M. tuberculosis*, slowed down further in the absence of acetamide (Fig. 3B). Although immunoblotting did not reveal any significant differences in FtsZ-GFP levels when the strain was grown with and without acetamide for four doublings (data not shown), the absence of inducer led to a 20% increase in average cell length (from 2.47 μm [n = 119] to 2.98 μm [n = 105]). Thus, growth in the absence of acetamide inhibited cell division and led to a reduction in the viability of *M. tuberculosis* 41. Therefore, loss of viability perhaps occurs before major changes in the FtsZ level become apparent. Furthermore, immunoblotting may not be sensitive enough to discern the small changes in FtsZ levels that are nevertheless able to affect the cell division of *M. tuberculosis* 41 grown in the absence of acetamide. Expression from the inducible amidase promoter is known to be leaky in *M. tuberculosis* (4, 9, 10, 15; our unpublished data). Since *M. tuberculosis* 41 required acetamide for viability, these data also suggest that the leaky expression is not sufficient to sustain the growth of this strain. Furthermore, growth in the absence of acetamide beyond four doublings may be required to see a reduction in FtsZ levels. Together, the above results confirm that FtsZ$_{TB}$-GFP is the only FtsZ protein produced in *M. tuberculosis* 41 and suggest that it is functional in *M. tuberculosis* cell division. It is pertinent to note that although merodiploid strains producing FtsZ-GFP fusion proteins have been

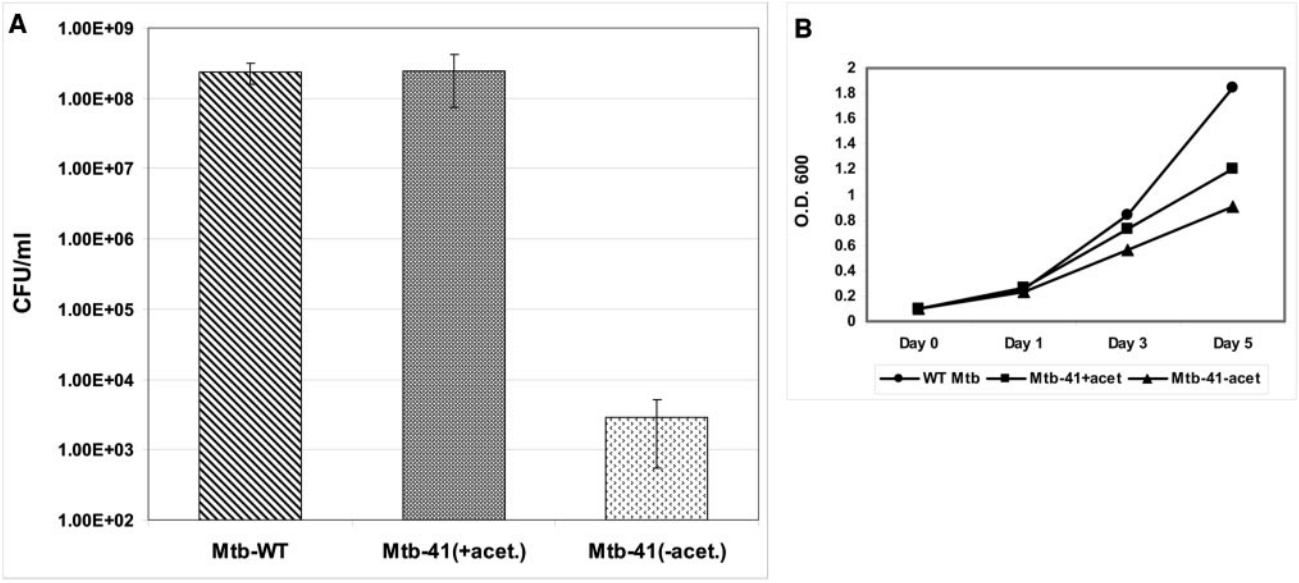

FIG. 3. *M. tuberculosis* 41 needs acetamide for growth. (A) Viability of *M. tuberculosis* 41. Actively growing cultures of wild-type (WT) *M. tuberculosis* or *M. tuberculosis* 41 were plated on 7H10 Middlebrook agar plates with or without 0.2% acetamide. Colony counts obtained after 3 weeks of incubation at 37°C are shown. Means and standard errors from three separate experiments are shown. (B) Growth of *M. tuberculosis* 41 in the presence or absence of acetamide. Exponentially growing cultures of *M. tuberculosis* 41 were washed two times with medium lacking acetamide, followed by growth in medium with (squares) or without (triangles) acetamide (acet.). For comparison, wild-type *M. tuberculosis* H37Ra was also grown (circles). Cultures were grown with shaking at 37°C, and their optical density at 600 nm (O.D. 600) was measured at the indicated times. Mtb, *M. tuberculosis*.

reported in other bacteria, efforts to utilize an *ftsZ* reporter strain where *ftsZ-gfp* functions as the sole source of *ftsZ* have met with limited success. For example, in *E. coli*, where *ftsZ* dynamics are well characterized at the genetic and biochemical levels, FtsZ-GFP is not fully capable of replacing the function of native FtsZ (20, 37). Similarly, fusion of the only copy of *ftsZ* to *gfp* in *Bacillus subtilis* resulted in a temperature-sensitive phenotype due, perhaps, to the inability of the fusion protein to fold properly at high temperature (17). In *Streptomyces coelicolor*, *ftsZ-gfp* is capable of complementing an *ftsZ* chromosomal null mutation but the resultant strain exhibits a delayed and defective sporulation phenotype (14).

Low frequency of Z rings in *M. tuberculosis*. Next, we visualized $FtsZ_{TB}$-GFP structures by fluorescence microscopy in actively growing cells of *M. tuberculosis* 41. The majority of cells with FtsZ-GFP structures had distinct midcell FtsZ bands (Fig. 4), although some cells had FtsZ localized at poles (arrows in Fig. 4a and c). Sometimes, cells with midcell Z rings showed faint polar fluorescence, and conversely, cells with distinct polar spots showed faint or incomplete Z rings. Approximately 11% of actively growing cells had midcell Z rings (Table 3). *M. tuberculosis* is a slow grower with an average doubling time of 24 h. Thus, the observed low frequency of midcell Z rings presumably reflects the actual percentage of cells undergoing cell division. It is pertinent to note that approximately 30% of actively growing *M. smegmatis ftsZ* merodiploid cells contain midcell Z rings (30, 31). Presumably, the frequency of Z-ring formation is proportional to the growth rate of mycobacteria. Growth rate-dependent changes in the frequency of medial Z rings have been reported for *B. subtilis* (18, 42). Recently, Erickson and colleagues measured fluorescence recovery after photobleaching of GFP-tagged FtsZ proteins of *E. coli* and *B. subtilis* and concluded that the Z ring is highly dynamic and continuously remodels itself with a half-time of 8 s (1, 35). It will be interesting to determine whether

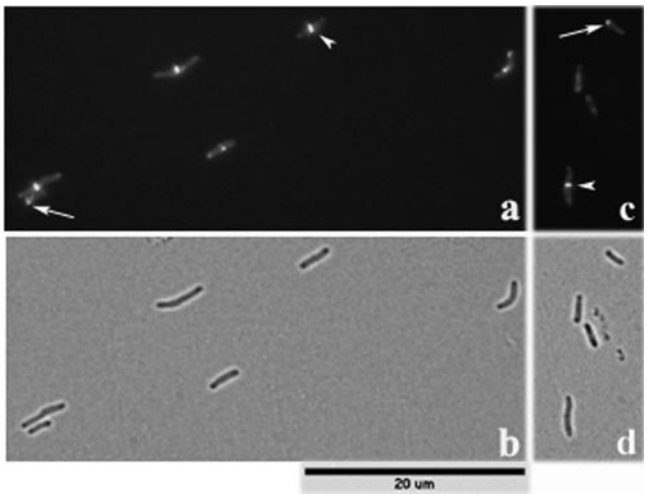

FIG. 4. Microscopy of *M. tuberculosis* 41. Actively growing cultures of *M. tuberculosis* 41 grown with 0.2% acetamide were examined by fluorescence (a and c) and bright-field (b and d) microscopy. Images were selected to show the shape, size, and FtsZ structures of as many cells as possible and therefore do not reflect the actual frequency of the various FtsZ structures seen (Table 3). Arrowheads and arrows indicate midcell FtsZ-GFP rings and polar FtsZ-GFP localization, respectively.

TABLE 3. Presence of Z rings in cells

Growth condition	No. of cells	No. of cells with FtsZ-GFP structures[b]	FtsZ-GFP structures		
			Midcell[c]	Polar	Others[a]
With acetamide	359	53 (14.7[f])[d]	38 (72)	15 (28)	3
Acetamide + SRI3072[e]	178	4 (2.2)	4 (2.2)	0	4

[a] Cells with either incomplete rings or rings in quarter position.
[b] Polar, midcell structures or others.
[c] Cells with complete midcell Z ring.
[d] Parentheses, percent cells with FtsZ-GFP structures.
[e] 48 h of exposure.
[f] 10.6% midcell + 4.1% polar.

the Z-ring assembly dynamics in slow growers such as *M. tuberculosis* are proportionately slower.

The average length of *M. tuberculosis* 41 cells with distinct polar structures was ~2.2 μm (N = 38), whereas that of the cells with evident midcell bands was 4.0 μm (N = 59). Since wild-type *M. tuberculosis* cells grown under similar conditions were ~2.1 μm (N = 100) in length, this approximately twofold increase suggested that the polar structures could be remnants of septa from the previous division event. The above interpretation assumes that the polar localizations of FtsZ were not unique to *M. tuberculosis* 41 and could be observed in the parent strain. Alternatively, it is possible that interactions of $FtsZ_{TB}$ and negative regulators of Z-ring assembly in *M. tuberculosis*, if any, were perturbed in *M. tuberculosis* 41, resulting in localization of FtsZ at non-midcell sites. We tend to favor the first interpretation because the average size of cells with polar localizations was similar to the average length of actively growing *M. tuberculosis* cells. Most cells showed dark coloration at the cell poles. While the exact nature of these dark spots is unclear, they could be due to the external ridges observed at the cell poles of *M. tuberculosis* by transmission electron microscopy (6).

Disassembly of Z rings by SRI-3072. Recently, a group of structurally diverse small-molecule inhibitors, named zantrins, was shown to perturb the Z-ring assembly in *E. coli* and inhibit the growth of several bacterial species in broth cultures. These compounds interfered with the GTPase activity of *E. coli* FtsZ ($FtsZ_{EC}$) and $FtsZ_{TB}$, caused destabilization of $FtsZ_{EC}$ protofilaments, increased filament stability, and in some cases interfered with Z-ring assembly (21). The effects of zantrins on *M. tuberculosis* growth and $FtsZ_{TB}$ assembly were not examined in these experiments. We (R.R.) recently showed that SRI-3072, a small-molecule inhibitor belonging to a class of 2-alkoxycarbonylaminopyridines, inhibited the growth of *M. tuberculosis* with an MIC of 250 ng/ml (0.47 μM) (44). This compound also inhibited the GTPase activity of $FtsZ_{TB}$ in vitro, albeit with low affinity (i.e., 20% reduction in activity at 100 μM). Since it was unknown whether SRI-3072 affected FtsZ polymerization and Z-ring assembly in vivo, we addressed this question with *M. tuberculosis* 41.

Actively growing cultures of *M. tuberculosis* 41 were exposed to 0.56 μM SRI-3072 for various times, and effects of the inhibitor on growth and $FtsZ_{TB}$ structures were examined. As expected, SRI-3072 interfered with the growth of *M. tuberculosis* 41 (Fig. 5A). Fluorescence microscopy revealed a gradual disappearance of Z rings (Fig. 5B, parts a, c, e, and g) with increasing times of exposure. After 24 h of exposure, a reduction in the number of cells containing midcell Z rings was noted, although FtsZ-GFP localization at random spots was evident (data not shown; Fig. 5B, parts e to h). After 48 h of exposure, FtsZ-GFP localization at random spots also became compromised and a small increase in cell length was noted (Fig. 5B and C). Midcell $FtsZ_{TB}$-GFP bands were present in approximately 2.2% of drug-treated cells, whereas they accounted for 11% in untreated controls (Table 3). By day 5, almost no distinct Z rings were evident; rather, only diffuse and faint fluorescence was seen in most cells (Fig. 5B, parts g and h). A modest increase in cell length combined with the disappearance of Z rings is consistent with the interpretation that SRI-3072 interfered with $FtsZ_{TB}$ ring assembly and cell division. It is pertinent to note that zantrins, which inhibit the growth of a wide range of bacteria, did not cause overt filamentation (21). In comparison to SRI-3072-treated cells, 4% of untreated cells had midcell Z rings after 120 h of growth (not shown). We have shown previously that the FtsZ levels in *M. tuberculosis* decrease during the stationary phase (9). The reduction in the number of cells with midcell Z rings at 120 h of growth presumably reflects the fact that these cells were in the stationary phase of growth. Treatment of *M. tuberculosis* 41 with SRI-3072 for 72 h caused an approximately 33% decrease in FtsZ levels, whereas no change in FtsZ levels was noted in untreated controls (data not shown). Interestingly, removal of SRI-3072 after 48 h of exposure did not result in recovery of viability (data not shown). It is possible that the compound SRI-3072 has inhibitory effects on other metabolic processes as well. The development and characterization of new antimycobacterial agents that affect *M. tuberculosis* proliferation are of great importance. The *M. tuberculosis* 41 reporter strain can potentially be used for evaluating the effects of new and reported inhibitors of $FtsZ_{TB}$ activities in vivo.

***M. tuberculosis* cells growing in macrophages are filamentous and deficient in midcell Z rings.** *M. tuberculosis* multiplication inside eukaryotic host cells is critical for virulence. It is unknown whether FtsZ assembly and cell division are affected during growth in macrophages. To begin addressing this issue, human macrophage-derived monocyte cell line THP-1 was infected with *M. tuberculosis* 41 and cultured for 3 days. We then recovered the intracellular bacteria and visualized them by fluorescence microscopy (Fig. 6). Results were compared with the cultures grown in broth. Two observations were readily apparent. First, macrophage-grown *M. tuberculosis* 41 cells were filamentous (Fig. 6C; compare parts i and ii with iii and iv) compared to broth-grown cultures, strongly suggesting a defect in cell division. The wild-type *M. tuberculosis* strain also

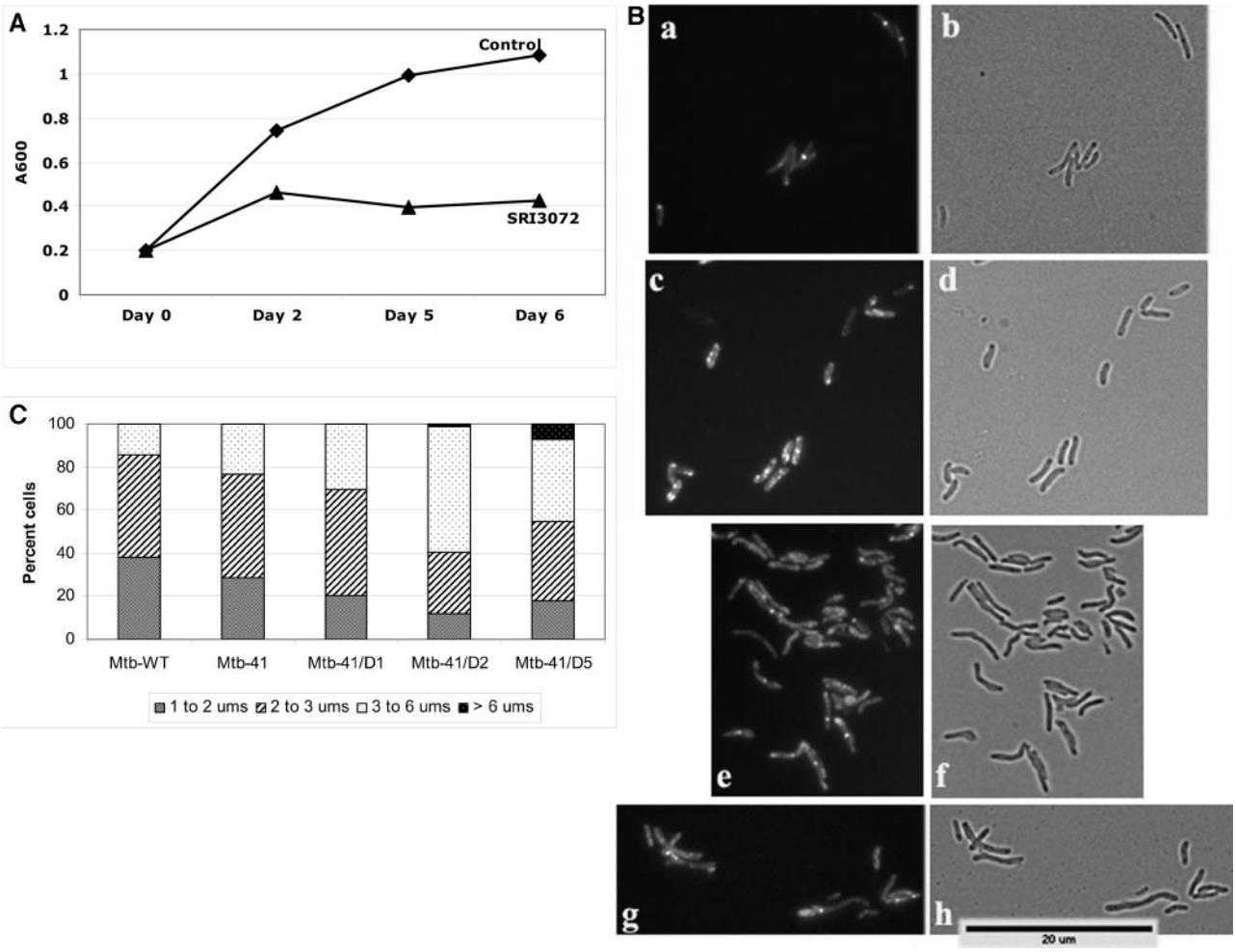

FIG. 5. SRI-3072 inhibits cell division and growth of *M. tuberculosis* 41. (A) Effect of SRI-3072 on growth of *M. tuberculosis* 41. Exponentially growing cultures of *M. tuberculosis* 41 were diluted to an optical density at 600 nm [OD (600 nm)] of 0.2 and grown in the presence or absence of 0.56 μM SRI-3072. The culture optical density at 600 nm was measured for up to 6 days and plotted. (B) Z-ring formation is inhibited by SRI-3072. *M. tuberculosis* 41 was grown in the presence of acetamide and 0.56 μM SRI-3072 for various periods of time and examined by fluorescence (a, c, e, and g) and bright-field (b, d, f, and h) microscopy. Images were captured, analyzed, and processed as described in Materials and Methods. Parts: a and b, no treatment; c and d, 24 h; e and f, 48 h; g and h, 120 h. (C) SRI-3072 inhibits cell division. Cell length measurements were made for untreated (*M. tuberculosis* wild type [WT], *M. tuberculosis* 41) and SRI-3072-treated *M. tuberculosis* 41 cells (*M. tuberculosis* 41/D1, *M. tuberculosis* 41/D2, and *M. tuberculosis* 41/D5). D1, D2, and D5 indicate 24, 48, and 120 h of treatment. At least 100 cells for each time point were measured with the Metamorph 6.2 software. Mtb, *M. tuberculosis*.

showed filamentation upon growth in THP-1 (Fig. 6A and B), indicating that the cell elongation phenotype is a characteristic feature of intracellular *M. tuberculosis*. Some filamentous cells also contained buds and bulges (Fig. 6C, arrowheads in parts iii and iv). Such structures were reported for *M. smegmatis* grown under conditions that increase FtsZ (10) or deplete WhmD (12). Second, fluorescence microscopy revealed that, in contrast to broth-grown cultures, a majority of macrophage-grown *M. tuberculosis* 41 cells had several nonring structures along the entire length of the cell, and only a small population of filamentous cells (1 to 3%) contained distinct Z rings at midcell sites (Fig. 6C, part iii). Processing of fluorescent images by the homomorphic FFT filtering function of the Metamorph 6.2 software revealed diffuse, spiral-like structures (Fig. 6D, parts i to vi). Because of the narrow width of *M. tuberculosis* cells, we did not succeed in improving the quality of these images to better discern the spiral structures. Since *M. tuberculosis* cells continue to proliferate in macrophages, we reasoned that these diffuse spiral structures were intermediates in FtsZ assembly (38) and would eventually lead to productive Z rings and subsequent cell division.

Localization of FtsZ in nonring structures has also been observed under FtsZ overproduction conditions in *E. coli* (20) and during sporulation in *B. subtilis* (2). Studies based on fluorescence recovery after photobleaching indicated that only 30% of the total FtsZ in *E. coli* is in the Z ring, with the rest in the cytoplasm (36). Time-lapse analysis of FtsZ structures indicated that FtsZ outside of the Z ring is in highly dynamic, potentially helical cytoskeletal structures (38). It was suggested that the highly mobile structures serve to scan the cell surface for potential division sites more efficiently. It remains to be established whether the diffuse, spiral-like structures observed

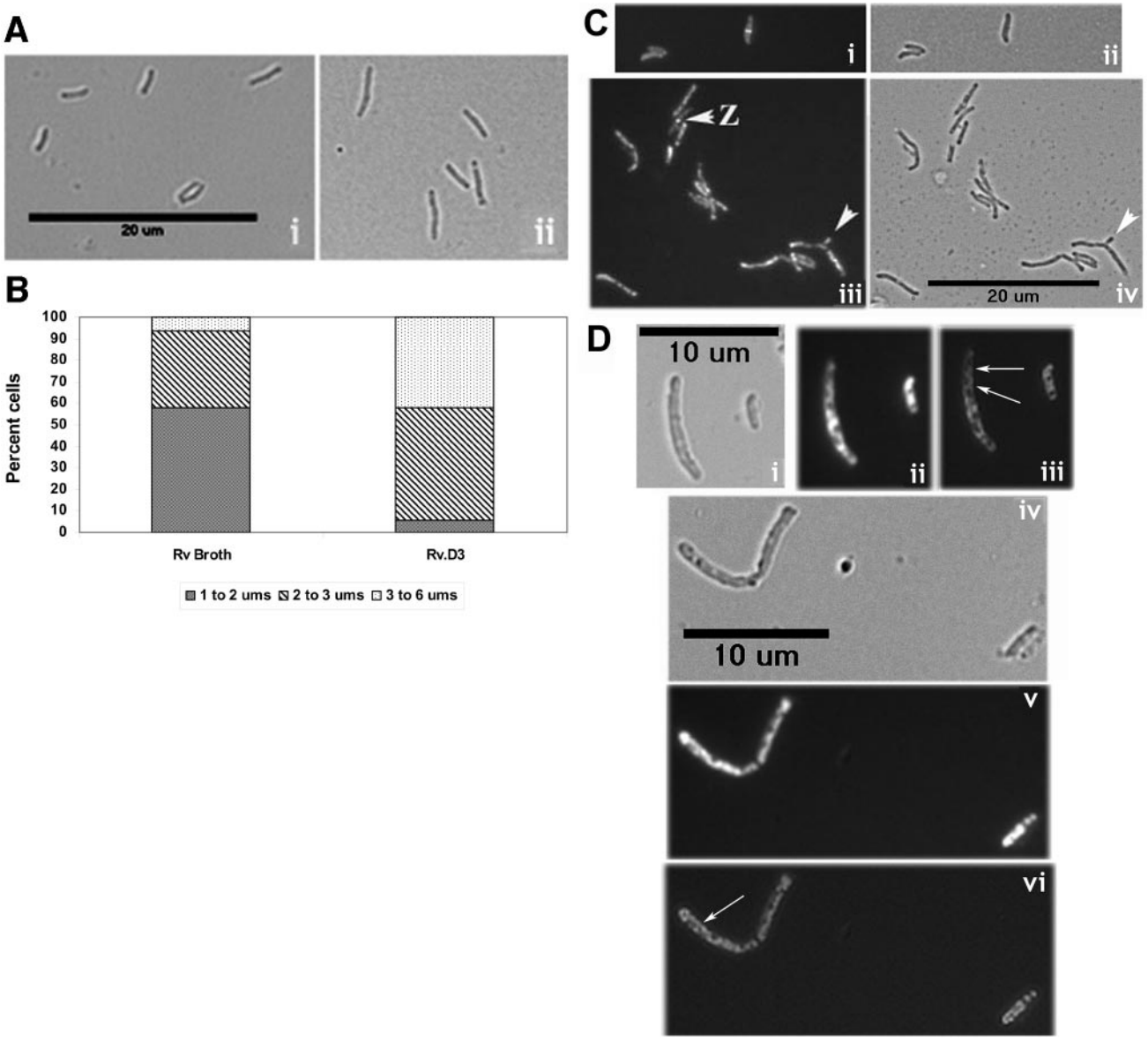

FIG. 6. Growth of *M. tuberculosis* in macrophages leads to filamentation. Wild-type *M. tuberculosis* or *M. tuberculosis* 41 was used to infect monolayers of gamma interferon-activated THP-1 macrophages at a multiplicity of infection of 1:10. After 3 h of incubation, unattached bacteria were washed off and macrophages were cultured for 72 h. Macrophages were then lysed and bacteria collected by centrifugation and examined by fluorescence and bright-field microscopy. (A) Macrophage-grown wild-type *M. tuberculosis*. Bright-field images of broth (i)- and macrophage (ii)-grown *M. tuberculosis* are shown. (B) Lengths of intracellular *M. tuberculosis* cells. Cell length measurements were made for broth-grown (RV Broth) and intracellular wild-type *M. tuberculosis* after 3 days (Rv.D3) of growth in THP-I cells. (C) Broth- and macrophage-grown *M. tuberculosis* 41. Fluorescence (i and iii) and bright-field (ii and iv) images of broth (i and ii)- and macrophage (iii and iv)-grown *M. tuberculosis* 41 are shown. Arrowheads indicate either bud-like structures or Z rings (Z). (D) Macrophage-grown *M. tuberculosis* cells show non-midcell localization of FtsZ. Fluorescence images of macrophage-grown *M. tuberculosis* 41 bacteria were manipulated with the FFT processing function of the Metamorph 6.2 software (see Materials and Methods). This revealed the presence of almost spiral-like structures of FtsZ-GFP along the length of the cells (arrows in parts iii and vi). Parts i and iv and parts ii and v are respective bright-field and fluorescence images. Images in parts iii and vi are FFT processed. Images in panel D are slightly enlarged to show the FtsZ-GFP structures more clearly.

during the intracellular growth of *M. tuberculosis* 41 cells are comparable to the well-characterized FtsZ structures of *E. coli* (38) and *B. subtilis* (2).

FtsZ levels in bacteria grown in macrophages or in broth are comparable. We considered whether the low frequency of Z rings at midcell sites during intracellular growth was due to altered levels of FtsZ. Cellular lysates from macrophage-grown bacteria were prepared and FtsZ levels were determined by immunoblotting with anti-$FtsZ_{TB}$ antibodies. Since protein lysates prepared from these bacteria could be contaminated with small amounts of macrophage proteins, FtsZ levels were normalized to those of SigA. The levels of SigA, a housekeeping sigma factor, are known to be stably maintained under various conditions of growth in broth and in vivo (13, 45). The immu-

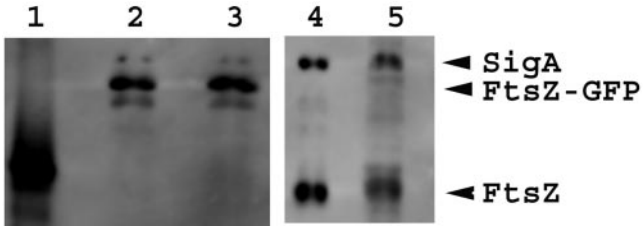

FIG. 7. FtsZ levels in macrophage-grown *M. tuberculosis*. Levels of $FtsZ_{TB}$ and $FtsZ_{TB}$-GFP in broth- and macrophage-grown bacteria were determined by immunoblotting. Cellular lysates of broth- and macrophage-grown bacteria were prepared as described in Materials and Methods. Bacterial pellet was lysed by bead beating, resolved by SDS-PA gel electrophoresis, transferred to nitrocellulose membranes, probed with anti-$FtsZ_{TB}$ and monoclonal anti-*E. coli* sigma 70 antibodies, and processed as previously described, with the ECF Western blotting kit from Amersham (12). In some cases, macrophages containing bacteria were pelleted and directly lysed by beat beating (lane 5) and processed as described above. Lanes: 1, recombinant $FtsZ_{TB}$ protein; 2, lysate from broth-grown *M. tuberculosis* 41; 3, lysate from macrophage-isolated *M. tuberculosis* 41; 4, lysate from broth-grown wild-type *M. tuberculosis*; 5, lysate from macrophage-grown wild-type *M. tuberculosis*. Note that lysates in lane 5 were obtained by bead beating macrophages containing wild-type *M. tuberculosis*, whereas for lane 3, bacteria were first recovered from macrophages by gentle lysis and then cellular lysates were prepared by bead beating. Although the former approach (lane 5) resulted in a slightly higher background level compared to the one in lane 3, the ratio of SigA to FtsZ was unaffected. Positions of SigA, $FtsZ_{TB}$, and $FtsZ_{TB}$-GFP are marked.

noblots were therefore probed simultaneously with anti-$FtsZ_{TB}$ and monoclonal anti-σ^{70} antibodies. Analysis by a fluorescence imager indicated that the ratio of FtsZ to SigA in lysates prepared from bacteria grown in macrophages was comparable to the ratio obtained for broth-grown bacteria (Fig. 7; data not shown).

Together, the above results suggested that the altered activities of FtsZ, and not the altered protein levels, were responsible for the observed nonring structures during intracellular growth. This raises a question as to why such nonring FtsZ structures were abundant during intracellular growth but were not readily detectable during growth in broth. We propose that the $FtsZ_{TB}$ assembly at the midcell site is regulated by a hitherto unidentified accessory factor(s) whose activity could be compromised or altered during intracellular growth, thereby resulting in diffuse nonring structures and filamentation. Based on the genome data, *M. tuberculosis* appears to lack orthologs of known regulators and stabilizers of Z-ring and FtsZ-interacting proteins. To date, the only interactions of $FtsZ_{TB}$ reported are those with $FtsW_{TB}$ (7). Although the FtsZ-FtsW interaction is critical for cell division, FtsZ can localize to the midcell site independently of FtsW (31). The intracellular environment that *M. tuberculosis* faces upon infection is believed to be hostile and rich in reactive nitrogen and oxygen intermediates, cytokines, and antimicrobial peptides. It is also acidic and hypoxic in nature and nutrient limited (34). *M. tuberculosis* adapts to the stressful intracellular environment by modulating the expression (34) of a wide array of genes, including perhaps those responsible for the observed diffuse FtsZ structures and filamentation. Presumably, the balance of proteins promoting and inhibiting Z-ring assembly is perturbed during growth of *M. tuberculosis* in macrophages. However, an alternate possibility, that FtsZ-GFP fusion protein is less stable and that filamentation caused by hitherto unknown mechanisms during intramacrophage growth readily disassembles midcell FtsZ-GFP rings, remains open. It should be noted that FtsZ-GFP spiral-like structures were evident during intramacrophage growth, although there was a reduction in the number of midcell FtsZ-GFP rings (Fig. 6). It is likely that the stability of FtsZ-GFP in spiral-like structures is different from that in midcell rings.

Bacterial filamentation is often triggered by a wide variety of factors, including exposure to DNA-damaging agents and to antibacterial agents that interfere with FtsI activity (recently reviewed in reference 24). Filamentation during intracellular growth has also been reported for some gram-negative pathogens. For example, *Salmonella enterica* serovar Typhimurium growing in murine fibroblast cells (23) and contractile vacuoles of amoebae (11), *S. enterica* in macrophages (39), and uropathogenic *E. coli* in superficial bladder epithelial cells (26) are all filamentous. It is, however, pertinent to note that the filamentous cells of *S. enterica* serovar Typhimurium have distinct FtsZ bands at presumptive midcell locations, and a defect in the histidine biosynthetic pathway is correlated with the observed filamentation phenotype (16). The filamentation phenotype of *M. tuberculosis* during intracellular growth suggests that the pathogen's cell division process is delayed in response to infection, and this delay could be attributed to compromised function of $FtsZ_{TB}$. Characterization of *M. tuberculosis* 41 should greatly help us to identify the factors that affect the cell division process during intracellular growth of *M. tuberculosis*.

ACKNOWLEDGMENTS

This work was supported in part by grants AI48417 (M.R.) and AI41406 (M.V.V.S.M.).

We thank Jaroslaw Dziadek for help with the construction of some plasmids and Zafer Hatahet, William Margolin, Harold P. Erickson, and Marianthi Coronéou for insightful comments and helpful suggestions.

REFERENCES

1. **Anderson, D. E., F. J. Gueiros-Filho, and H. P. Erickson.** 2004. Assembly dynamics of FtsZ rings in *Bacillus subtilis* and *Escherichia coli* and effects of FtsZ-regulating proteins. J. Bacteriol. **186:**5775–5781.
2. **Ben-Yehuda, S., and R. Losick.** 2002. Asymmetric cell division in B. subtilis involves a spiral-like intermediate of the cytokinetic protein FtsZ. Cell **109:** 257–266.
3. **Bramhill, D.** 1997. Bacterial cell division. Annu. Rev. Cell Dev. Biol. **13:** 395–424.
4. **Carroll, P., D. G. Muttucumaru, and T. Parish.** 2005. Use of a tetracycline-inducible system for conditional expression in *Mycobacterium tuberculosis* and *Mycobacterium smegmatis*. Appl. Environ. Microbiol. **71:**3077–3084.
5. **Cormack, B. P., R. H. Valdivia, and S. Falkow.** 1996. FACS-optimized mutants of the green fluorescent protein (GFP). Gene **173:**33–38.
6. **Dahl, J. L.** 2004. Electron microscopy analysis of Mycobacterium tuberculosis cell division. FEMS Microbiol. Lett. **240:**15–20.
7. **Datta, P., A. Dasgupta, S. Bhakta, and J. Basu.** 2002. Interaction between FtsZ and FtsW of Mycobacterium tuberculosis. J. Biol. Chem. **277:**24983–24987.
8. **Dye, C., S. Scheele, P. Dolin, V. Pathania, and M. C. Raviglione.** 1999. Consensus statement. Global burden of tuberculosis: estimated incidence, prevalence, and mortality by country. WHO Global Surveillance and Monitoring Project. JAMA **282:**677–686.
9. **Dziadek, J., M. V. Madiraju, S. A. Rutherford, M. A. Atkinson, and M. Rajagopalan.** 2002. Physiological consequences associated with overproduction of Mycobacterium tuberculosis FtsZ in mycobacterial hosts. Microbiology **148:**961–971.
10. **Dziadek, J., S. A. Rutherford, M. V. Madiraju, M. A. Atkinson, and M. Rajagopalan.** 2003. Conditional expression of Mycobacterium smegmatis ftsZ, an essential cell division gene. Microbiology **149:**1593–1603.
11. **Gaze, W. H., N. Burroughs, M. P. Gallagher, and E. M. Wellington.** 2003. Interactions between Salmonella typhimurium and Acanthamoeba polyphaga, and observation of a new mode of intracellular growth within contractile vacuoles. Microb. Ecol. **46:**358–369.

12. **Gomez, J. E., and W. R. Bishai.** 2000. whmD is an essential mycobacterial gene required for proper septation and cell division. Proc. Natl. Acad. Sci. USA **97:**8554–8559.
13. **Gomez, M., L. Doukhan, G. Nair, and I. Smith.** 1998. sigA is an essential gene in Mycobacterium smegmatis. Mol. Microbiol. **29:**617–628.
14. **Grantcharova, N., U. Lustig, and K. Flardh.** 2005. Dynamics of FtsZ assembly during sporulation in *Streptomyces coelicolor* $A3_2$. J. Bacteriol. **187:**3227–3237.
15. **Greendyke, R., M. Rajagopalan, T. Parish, and M. V. Madiraju.** 2002. Conditional expression of Mycobacterium smegmatis dnaA, an essential DNA replication gene. Microbiology **148:**3887–3900.
16. **Henry, T., F. Garcia-Del Portillo, and J. P. Gorvel.** 2005. Identification of Salmonella functions critical for bacterial cell division within eukaryotic cells. Mol. Microbiol. **56:**252–267.
17. **Levin, P. A., I. G. Kurtser, and A. D. Grossman.** 1999. Identification and characterization of a negative regulator of FtsZ ring formation in Bacillus subtilis. Proc. Natl. Acad. Sci. USA **96:**9642–9647.
18. **Lin, D. C., P. A. Levin, and A. D. Grossman.** 1997. Bipolar localization of a chromosome partition protein in Bacillus subtilis. Proc. Natl. Acad. Sci. USA **94:**4721–4726.
19. **Lowe, J.** 1998. Crystal structure determination of FtsZ from Methanococcus jannaschii. J. Struct. Biol. **124:**235–243.
20. **Ma, X., D. W. Ehrhardt, and W. Margolin.** 1996. Colocalization of cell division proteins FtsZ and FtsA to cytoskeletal structures in living Escherichia coli cells by using green fluorescent protein. Proc. Natl. Acad. Sci. USA **93:**12998–13003.
21. **Margalit, D. N., L. Romberg, R. B. Mets, A. M. Hebert, T. J. Mitchison, M. W. Kirschner, and D. RayChaudhuri.** 2004. Targeting cell division: small-molecule inhibitors of FtsZ GTPase perturb cytokinetic ring assembly and induce bacterial lethality. Proc. Natl. Acad. Sci. USA **101:**11821–11826.
22. **Margolin, W.** 2000. Themes and variations in prokaryotic cell division. FEMS Microbiol. Rev. **24:**531–548.
23. **Martinez-Moya, M., M. A. de Pedro, H. Schwarz, and F. Garcia-del Portillo.** 1998. Inhibition of Salmonella intracellular proliferation by non-phagocytic eucaryotic cells. Res. Microbiol. **149:**309–318.
24. **Miller, C., L. E. Thomsen, C. Gaggero, R. Mosseri, H. Ingmer, and S. N. Cohen.** 2004. SOS response induction by beta-lactams and bacterial defense against antibiotic lethality. Science **305:**1629–1631.
25. **Mukherjee, A., and J. Lutkenhaus.** 1998. Dynamic assembly of FtsZ regulated by GTP hydrolysis. EMBO J. **17:**462–469.
26. **Mulvey, M. A., J. D. Schilling, and S. J. Hultgren.** 2001. Establishment of a persistent *Escherichia coli* reservoir during the acute phase of a bladder infection. Infect. Immun. **69:**4572–4579.
27. **Parish, T., and N. G. Stoker.** 2000. Use of a flexible cassette method to generate a double unmarked Mycobacterium tuberculosis tlyA plcABC mutant by gene replacement. Microbiology **146**(Pt. 8)**:**1969–1975.
28. **Pashley, C. A., and T. Parish.** 2003. Efficient switching of mycobacteriophage L5-based integrating plasmids in Mycobacterium tuberculosis. FEMS Microbiol. Lett. **229:**211–215.
29. **Predich, M., L. Doukhan, G. Nair, and I. Smith.** 1995. Characterization of RNA polymerase and two sigma-factor genes from Mycobacterium smegmatis. Mol. Microbiol. **15:**355–366.
30. **Rajagopalan, M., M. A. Atkinson, H. Lofton, A. Chauhan, and M. V. Madiraju.** 2005. Mutations in the GTP-binding and synergy loop domains of Mycobacterium tuberculosis ftsZ compromise its function in vitro and in vivo. Biochem. Biophys. Res. Commun. **331:**1171–1177.
31. **Rajagopalan, M., E. Maloney, J. Dziadek, M. Poplawska, H. Lofton, A. Chauhan, and M. V. Madiraju.** 2005. Genetic evidence that mycobacterial FtsZ and FtsW proteins interact, and colocalize to the division site in Mycobacterium smegmatis. FEMS Microbiol. Lett. **250:**9–17.
32. **Romberg, L., and P. A. Levin.** 2003. Assembly dynamics of the bacterial cell division protein FTSZ: poised at the edge of stability. Annu. Rev. Microbiol. **57:**125–154.
33. **Sambrook, J., E. F. Fritsch, and T. Maniatis.** 1989. Molecular cloning: a laboratory manual, 2nd ed. Cold Spring Harbor Laboratory Press, Cold Spring Harbor, N.Y.
34. **Schnappinger, D., S. Ehrt, M. I. Voskuil, Y. Liu, J. A. Mangan, I. M. Monahan, G. Dolganov, B. Efron, P. D. Butcher, C. Nathan, and G. K. Schoolnik.** 2003. Transcriptional adaptation of Mycobacterium tuberculosis within macrophages: insights into the phagosomal environment. J. Exp. Med. **198:**693–704.
35. **Stricker, J., and H. P. Erickson.** 2003. In vivo characterization of *Escherichia coli ftsZ* mutants: effects on Z-ring structure and function. J. Bacteriol. **185:**4796–4805.
36. **Stricker, J., P. Maddox, E. D. Salmon, and H. P. Erickson.** 2002. Rapid assembly dynamics of the Escherichia coli FtsZ-ring demonstrated by fluorescence recovery after photobleaching. Proc. Natl. Acad. Sci. USA **99:**3171–3175.
37. **Sun, Q., and W. Margolin.** 1998. FtsZ dynamics during the division cycle of live *Escherichia coli* cells. J. Bacteriol. **180:**2050–2056.
38. **Thanedar, S., and W. Margolin.** 2004. FtsZ exhibits rapid movement and oscillation waves in helix-like patterns in Escherichia coli. Curr. Biol. **14:**1167–1173.
39. **Vazquez-Torres, A., Y. Xu, J. Jones-Carson, D. W. Holden, S. M. Lucia, M. C. Dinauer, P. Mastroeni, and F. C. Fang.** 2000. Salmonella pathogenicity island 2-dependent evasion of the phagocyte NADPH oxidase. Science **287:**1655–1658.
40. **Wayne, L. G.** 1994. Dormancy of Mycobacterium tuberculosis and latency of disease. Eur. J. Clin. Microbiol. Infect. Dis. **13:**908–914.
41. **Wayne, L. G., and C. D. Sohaskey.** 2001. Nonreplicating persistence of mycobacterium tuberculosis. Annu. Rev. Microbiol. **55:**139–163.
42. **Weart, R. B., and P. A. Levin.** 2003. Growth rate-dependent regulation of medial FtsZ ring formation. J. Bacteriol. **185:**2826–2834.
43. **White, E. L., L. J. Ross, R. C. Reynolds, L. E. Seitz, G. D. Moore, and D. W. Borhani.** 2000. Slow polymerization of *Mycobacterium tuberculosis* FtsZ. J. Bacteriol. **182:**4028–4034.
44. **White, E. L., W. J. Suling, L. J. Ross, L. E. Seitz, and R. C. Reynolds.** 2002. 2-Alkoxycarbonylaminopyridines: inhibitors of Mycobacterium tuberculosis FtsZ. J. Antimicrob. Chemother. **50:**111–114.
45. **Wu, S., S. T. Howard, D. L. Lakey, A. Kipnis, B. Samten, H. Safi, V. Gruppo, B. Wizel, H. Shams, R. J. Basaraba, I. M. Orme, and P. F. Barnes.** 2004. The principal sigma factor sigA mediates enhanced growth of Mycobacterium tuberculosis in vivo. Mol. Microbiol. **51:**1551–1562.